Solar Atmosphere Wave Dynamics Generated by Solar Global Oscillating Eigenmodes

M.K.Griffiths[1,1,], V.Fedun[1], R.Erdélyi[1]

[a]*Solar Physics and Space Plasma Research Centre (SP²RC), School of Mathematics and Statistics, University of Sheffield, Hicks Building, Hounsfield Road, S7 3RH, UK*
[b]*Corporate Information and Computing Services, The University of Sheffield, 10-12 Brunswick Street, Sheffield, S10 2FN, UK*
[c]*Department of Automatic Control and Systems Engineering, The University of Sheffield, Mappin Street, Sheffield, S1 3JD, UK*

Abstract

The solar atmosphere exhibits a diverse range of wave phenomena one of the earliest to be discovered was the five minute oscillation, the p-mode. The analysis of wave propagation in the solar atmosphere may be used as a diagnostic tool to measure the physical characteristics of the suns atmospheric layers.

In this paper we investigated the dynamics and propagation of waves which are generated by the solar global eigenmodes. We report on a series of hydrodynamic simulations of a realistic model of the solar atmosphere. With the objective of recreating atmospheric motions generated by global resonant oscillation the simulations use a driver which is spatially structured and extended in a sinusoidal profile across the computational model. The drivers perturb the region at 0.5Mm above the bottom boundary of the model and coincident with the temperature minimum. A combination of the VALIIIC and McWhirter solar atmospheres and coronal density profiles were used as the background equilibrium model in the simulations. We report on a study of synthetic photospheric oscillations for a magnetic field free model of the quiet sun. To carry out the simulations, we employed the MHD code, SMAUG (Sheffield MHD Accelerated Using GPUs).

Our results show that the amount of energy propagated into the solar atmosphere is consistent with a model of solar global oscillations described using the Klein-Gordon equation. The calculated results indicate a power law consistent with observational results obtained using SDO AIA **?**. Our results demonstrate the conversion of modes with a period of 30s to a mode with a period of 180s, demonstrating the Chromosphere may be a source of 180s oscillation modes. The results inidicate a shift in frequency arising from interference between the driven waves and reflections from the transition layer.

Keywords: magnetohydrodynamics (MHD); oscillations; MHD waves; solar atmosphere

*Corresponding author at: Corporate Information and Computing Services, The University of Sheffield, 10-12 Brunswick Street, Sheffield, S10 2FN, UK.
e-mail address: m.griffiths@sheffield.ac.uk

1. Introduction

The highly magnetised solar atmosphere exhibits a diverse range of wave phenomena. **?** reported the first observations of oscillatory behaviour with vertical motions on the solar surface, an amplitude of 300-400m/s and a period of 296s observations of Ca K band. These ubiquitous oscillations are referred to as the p-modes i.e. standing acoustic waves in the solar interior were explained by **?**. **?** reported analysis indicating that the vertical wavelength is comparable to the horizontal wavelength and is roughly 1000-5000km. There is a significant body of works reporting on observational, theoretical and computational studies of p-mode phenomena. The main restoring force for these modes of oscillation is the pressure, the 5 minute oscillation is the main manifestation of these modes. The detection of oscillations in the apparent solar diameter (see **?** and **?**) was one of the first suggestions of the truly global oscillations of the sun. The work of Christensen-Dalsgaard modelling solar oscillations on the basis of the solar structure provided spectra consistent with those of **?**, this was the start of helioseismology. Wave propagation in a medium such as the gravitationally stratified solar atmosphere results in the occurence of eigen-oscillations, these oscillations result from the internal interactions of the system. A model for understanding these oscillations can be understood from the normal mode solutions of the gravitating hydrodynamic slab in ideal MHD **?**. The solar p-modes are generated by global resonant oscillations, periodic and turbulent motions just beneath the photosphere. These resonant modes are reflected at the surface by the steep change in density. The increase of the sound speed causes refraction. The resulting propagation of this wave energy into the solar atmosphere may be used as a diagnostic tool to understand the physical characteristics of the solar atmospheric layers. We report on a series of hydrodynamical simulations modelling a realistic temperature, pressure and density solar atmosphere using a driver located at the temperature minimum mimicing the the various p-modes, the driver is extended in a sinusoidal profile arcoss the base of the computational model. The objectives of this work is to recreate the atmospheric motions generated by the global resonant oscillation, to understand how the energy provided by different modes of oscillation are redistributed in the solar atmosphere and to shed light on the mechanisms which lead to ubiquitous intensity oscillations in the solar atmosphere.

Observational and theoretical analysis generally describes mechanisms for the propagation of energy into the Chromosphere, into the Solar Corona or between the transition region and the Corona. We briefly summarise some of this work here. The growing field of coronal seismology uses the observed solar atmospheric wave modes to determine the physical characterisitcs of the solar atmosphere. This in turn requires a thorough understanding of the physics of the solar atmosphere. Although there is overwhelming evidence for photospheric 5 minute p-modes and 3 minute Chromospheric modes, the detection and characterisation of oscillatory phenomena in the corona are rare and difficult to detect. This makes the solution of the coronal heating problem more challenging. However, since the advent of Coronal Seismology (e.g. see **?** **?**) many spaced based high resolution solar observations e.g. SOHO, TRACE and SDO have provided evidence for wave phenomena in the solar atmosphere. The work of **?** provides a detailed study of intensity oscillations in the solar atmosphere. Using SDO/AIA data they study image sequences at somlar minimum and maximum for diffrent solar regions e.g. active regions, quiet sun and a coronal hole. The authors consider a lower coronal channel,

hot coronal channel and a cooler coronal channel. The study revealed strong 3-5 minute oscillations in all channels and included some longer period modes. The results indicated that diffrences my arise when the size of the area of observation is changed.The ubiquity of the observed 3 and 5 minute oscillations in all channels and regions is an indication of a global excitation mechanism.

Imagery from SDO 171$\mathring{A}$ and 193$\mathring{A}$ was used by **?** to compute the Fourier power spectra in the solar Corona. By analysing wave propagation in four regions of the solar atmosphere with different characteristics, they found that the distribution obeys a power law at low frequencies and possesses a flat distribution at high frequencies. This contrasts with the idea of a Gaussian noise distribution and a long time scale background. The implication is that this is the result of solar atmospheric heating from everywhere by small energy deposition events. It is expected that further measurements will constrain computational models.

Evidence for the upward propagation of acoustic wave with increasing amplitude has been demonstrated through a studies of variation in the intensities of Chromospheric lines for example the Ca lines at 854 nm (see **?**). Although the observed variations are unlikely to provide temperature rises observed in the Chromosphere they are a clear indication of the increase in dynamical activity from the photosphere to the chromosphere. The analysis of observations from the Observatorio del Teide/Tenerife by **?**, find that at a height of 250 km there is an acoustic energy flux of 3000 W/m2 2/3 of this energy is propagated by waves in the frequency range 5-10 mHz, the remaining third is carried by waves in the frequency range 10-20mHz. Waves with frequencies greater than the acoustic cut-off of 190s can contribute to the heating of the solar chromosphere. Reporting on measurements from the the Fe I 5434 $\mathring{A}$ **?** detect waves with periods down to 40s. For periods below the cutoff of 190s 40

Using the IMAX instrument on the sunrise observatory, **?** reported evidence for the excitation of solar acoustic oscillations excited by turbulent flows in the dark intergranular lanes. Individual sunquakes with epicenters near the solar surface and located in the intergranular lanes, are assumed to feed continuously energy into the resonant p-modes of the Sun and provide sources for acoustic oscillations. **?** presents wavefronts rippling near a granule and oriented along the direction of the intergranular lane. Using simultaneous observations of the Na and K lines with Doppler measurements **?** shows that inclined magnetic field lines provide portals along which magnetoacoustic energy can propagate at the intergranular boundaries.

There is a large body of computational work already undertaken to understand the propagation of waves in the solar atmosphere. Computational studies such as the study of Among others the following **?** et al study the Oscillatory Response of the 3D Solar Atmosphere to the Leakage of Photospheric Motion results are discussed in detail: i) High-frequency waves are shown to propagate from the lower atmosphere across the transition region, experiencing relatively low reflection, and transmitting most of their energy into the corona; ii) the thin transition region becomes a wave guide for horizontally propagating surface waves for a wide range of driver periods, and particularly at those periods that support chromospheric standing waves; iii) the magnetic field acts as a waveguide for both high- and low-frequency waves originating from the photosphere and propagating through the transition region into the solar corona. Previous work has considered either point source drivers with a gaussian velocity distribution. Other work e.g. **?** has demontrated that a strong initial pulse may lead to the quasi periodic rising of

chromospheric material into the lower corona in the form of spicules **?**. **?** considered the propagation of acoustic modes in a stratified hydrodynamical model of the solar atmosphere, they employed a cylindrically symmetric driver with a diameter of approximately 1Mm. They conclude that for driving regions of sizes smaller than the atmospheric scale height they are able to reproduce expansion waves which are characteristic of Chromospheric bright points. With a weak horizontal magnetic field, the physics within the interior of supergranulation cells **?** is suitably simple for undertaking hydrodynamic modelling. These modes ARE some sort of global eigenmodes, the coherence length of eigenoscillations at the photoshphere is 4Mm, and the power peaks at 5 mins.

2. Numerical Computation Methods

The 3D numerical simulations described here were undertaken using SMAUG, the GPU implementation of the Sheffield Advanced Code (SAC)**??**. SAC and SMAUG are numerical MHD solvers allowing us to model the time-dependent evolution of photospheric oscillations in the solar atmosphere. With the upper boundary of our model in the solar corona and the lower boundary in the photosphere the SMAUG code is well suited for modelling the leakage of wave energy from the photopshere, through the transition region and into the corona. We used open boundary conditions for the lower and upper boundaries which allowed us to model wave propagation for time scales characterised by the 5 minute p-mode induced oscillations. The general system of MHD equations are

$$\frac{\partial \rho}{\partial t} + \nabla \cdot (\mathbf{v}\rho) = 0, \tag{1}$$

$$\frac{\partial (\rho \mathbf{v})}{\partial t} + \nabla \cdot (\mathbf{v}\rho\mathbf{v} - \mathbf{B}\mathbf{B}) + \nabla p_t = \rho \mathbf{g}, \tag{2}$$

$$\frac{\partial e}{\partial t} + \nabla . (\mathbf{v}e - \mathbf{B}\mathbf{B} \cdot \mathbf{v} + \mathbf{v}p_t) + \nabla p_t = \rho \mathbf{g} \cdot \mathbf{v}, \tag{3}$$

$$\frac{\partial \mathbf{B}}{\partial t} + \nabla \cdot (\mathbf{v}\mathbf{B} - \mathbf{B}\mathbf{v}) = 0. \tag{4}$$

In these equations ρ is the mass density, $\mathbf{v}$ is the velocity, $\mathbf{B}$ is the magnetic field, e is the energy density, p_t is the total pressure and $\mathbf{g}$ is the gravitatioanl acceleration vector.

The total pressure p_t is written as

$$p_t = p_k + \frac{\mathbf{B}^2}{2}, \tag{5}$$

where p_k is the kinetic pressure given by

$$p_k = (\gamma - 1)(e - \frac{\rho \mathbf{v}^2}{2} - \frac{\mathbf{B}^2}{2}). \tag{6}$$

The equations (**??**) to (**??**) are applicable to an ideal compressible plasma. The SAC code is based on perturbed versions of these equations, thus the variables ρ, e and $\mathbf{B}$ are expressed in terms of perturbed and background quantities as

$$\rho = \tilde{\rho} + \rho_b, \tag{7}$$

$$e = \tilde{e} + e_b, \tag{8}$$

$$\mathbf{B} = \tilde{\mathbf{B}} + \mathbf{B}_b. \tag{9}$$

where $\tilde{\rho}$ is the perturbed density, $\tilde{e}$ is the perturbed energy and $\tilde{\mathbf{B}}$ is the perturbed magnetic field. The background quantities with a subscript b do not change in time, as we assume a magneto-hydrostatic equilibrium of the background plasma which may have a gravitational field present, denoted by $\mathbf{g}$. Hyper-diffusion and hyper-resistivity are implemented to achieve numerical stability of the computed solution of the MHD equations (see for example **?**). The full set of MHD equations, including the hyper-diffusion source terms are given in **?** and **?**.

3. Solar Atmospheric Model

In order oscillatory phenomena in the Solar Corona a physically representative model of the solar atmosphere is needed. An option is the use of a parametrisation of the tempearture of the solar atmosphere which may be a smoothed step function profile **?**. Results have demonstrated the need for observationally derived semi-emprical models of the solar atmosphere. There is much discussion about model validity and the work undertaken to demonstrate the reliability of the assumptions used to construct realistic models of the solar chromosphere **?**, **?**. The contention arises from the dynamical nature of the solar chromosphere for example local dynamo action has been suggested as a mechanism of Joule heating in the solar chromosphere **?**. The model atmosphere employed here is an observationally derived semi-empirical representation of the quiet sun. With the fundamental assumption of hydrostatic equilibrium a model of the chromosphere in equilibrium is constructed using the VALIIIc model, see **?**. For the region of the solar atmosphere above 2.5Mm the results of the energy balance model of solar coronal heating has been used (see **?**), this model includes an acoustic contribution comparable to the hydrostatic pressure. The corresponding temperature and density profiles are shown in figure 1.

4. Numerical Drivers for p-Mode Oscillations

For this study the model requires a driver mimicing the solar global oscillations. The overview of observational studies identified a range of physical phenomena resulting in oscillatory behaviour and delivering energy into the solar atmosphere. The results presented here extend earlier work undertaken by **?**, for their study point drivers were used to represent periodic buffeting or turbulent motions in the photosphere. The point driver is described by (**??**)

$$V_z = A \sin\left(\frac{2\pi t}{T_s}\right) \exp\left(\frac{-(x-x_0)^2}{\Delta x^2}\right) \exp\left(\frac{-(z-z_0)^2}{\Delta z^2}\right), \tag{10}$$

this driver has width Δx of 4Mm and width Δz of 4km and was applied to a 2D model of the realistic solar atmosphere. The results of the study demonstrated surface wave phenomena and structures in the transition region and highlighted the characteristics of the oscillatory phenomena as a result of frequency cutoffs induced by the stratified solar atmosphere. In contrast to the previous models we perturbed the whole boundary of

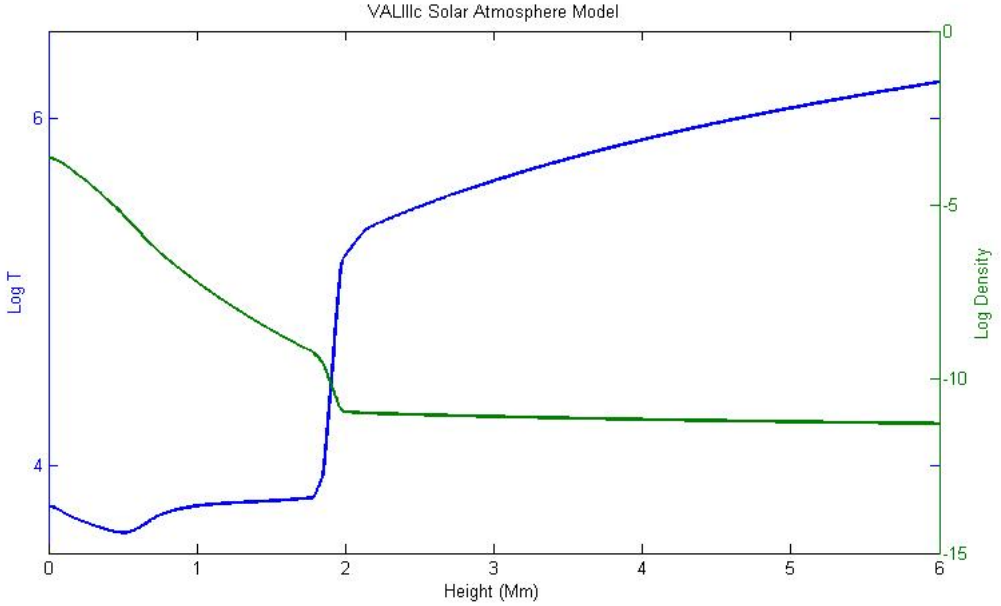

Figure 1: Temperature and density profiles used for the model atmosphere.

the model. In the real Sun, photospheric p-mode oscillations have a horizontal wavelength and coherence. Here, these excitations are represented with a vertical velocity driver located at the photosphere, this acoustic p-mode driver excites waves which propagate into a realisitc 3D model of the Solar atmosphere. Drivers representing different modes are considered, for example an extended driver with a sinusoidal dependence and a wavelength of 8Mm applied along the middle of the base of a computational domain of dimension 4Mm represents a fundamental mode. A driver with wavelength 4Mm applied the same way represents the first harmonic a "second harmonic" with wavelength 2Mm was also considered. Drivers may be constructed as an ensemble of these solar global eigenmodes. The vertical location of this extended driver is the temperature minimum which is 0.5Mm above the lower boundary of the model i.e. the photosphere. Such a driver may be represented by an equation (**??**) such as

$$V_z = A_{nm} \sin\left(\frac{2\pi t}{T_s}\right) \sin\left(\frac{(n+1)\pi x}{L_x}\right) \sin\left(\frac{(m+1)\pi y}{L_y}\right) \exp\left(\frac{-(z-z_0)^2}{\Delta z^2}\right), \qquad (11)$$

where the mode is defined by the index n and m in equation (**??**) and (**??**). Since we are investigating the leakage of energy into the solar atmosphere, for consistency it is necessary to ensure that for the different modes the driver amplitude is set to a value which provides the same total amount of energy over the model cross section and per unit time. For the n, m mode the energy, E_{nm} as a functionof z and time may be written as;

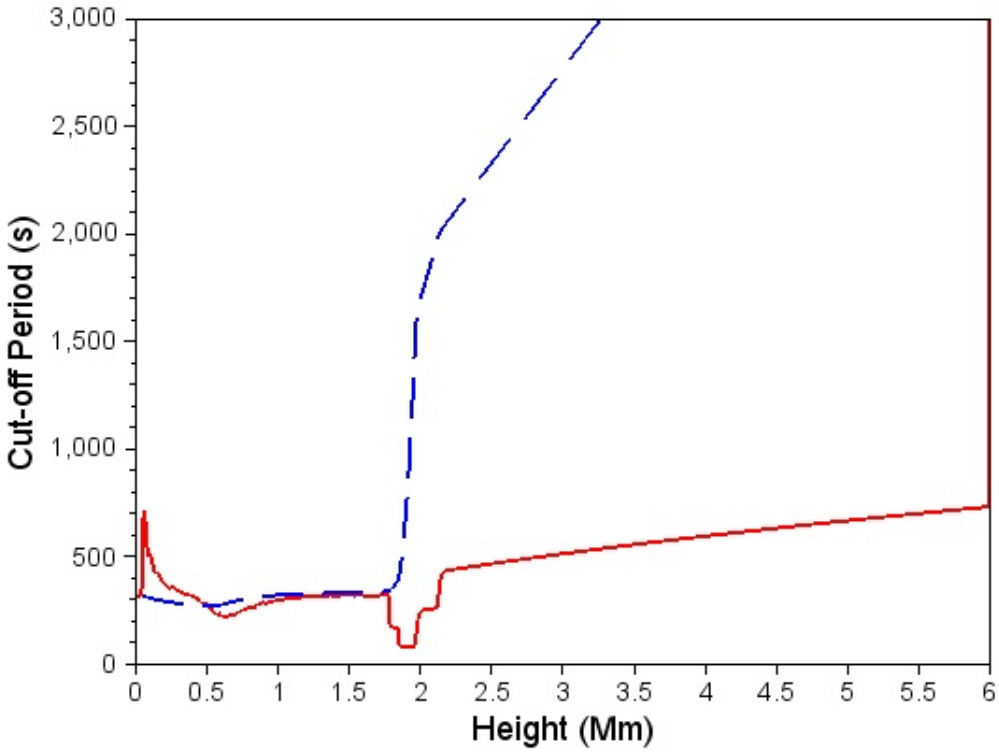

Figure 2: Cut off frequency at different heights in the model solar atmosphere.

$$E_{nm}(z,t) = \rho A_{nm}^2 I_{nm} \sin\left(\frac{2\pi t}{T_s}\right)^2 \exp\left(\frac{-(z-z_0)^2}{\Delta z^2}\right)^2, \tag{12}$$

I_{nm} is,

$$I_{nm} = \int_{-L_x}^{L_x}\int_{L_y}^{+L_y} \sin\left(\frac{(n+1)\pi x}{L_x}\right)^2 \sin\left(\frac{(m+1)\pi y}{L_y}\right)^2. \tag{13}$$

It is necessary to determine the amplitude A_{mn} for the different modes n, m with driver period T_s. This is achieved by computing the membrane energy integrated over the surface area and over a period of time from $t = 0$ to $t = T_m$ where T_m will correspond to the period of the driver with the largest value for the period. Following **?**, for the fundamental mode with driver period 300s, we set A_{00}=350ms^{-1}. Using the expression (**??**) to derive the ratio of the membrane energy for the mode n, m with driver period T_s, the mode (0,0) with driver period T_{00} and

set	description
a	Modes for the 30s, 180s and 300s Driver.
b	Normal Modes corresponding to different values of c_s
c	Normal Modes for equal mode values (i.e. n=m)

Table 1: Sets of simulations used to characterise oscillatory motions arising from an extended photospheric driver.

making $L_x = L_y$ gives the relation

$$A_{nm}^2 = \frac{2A_{00}^2 T_{rat}}{(n^2 + m^2 + 2(n+m) + 2)}.$$

$\mathrm{T}_m - \frac{T_{00}}{4\pi}\sin(\frac{4\pi T_m}{T_{00}})T_m - \frac{T_s}{4\pi}\sin(\frac{4\pi T_m}{T_s})(14)$

This relation was used to determine the amplitudes for the higher order modes, starting from the A_{00} mode we used $A_{00} = 350ms^{-1}$.

5. Numerical Analysis

Hydrodynamic simulations have been undertaken for a selection of drivers covering a range of time periods, modes and amplitudes supplying the same amount of energy, see (**??**). For this investigation we have been guided by the requirement that different driver modes deliver the same total amount of energy over the model cross section and when integrated over a time interval corresponding to the period of the longest period driver used for the set of simulations. Three sets of simulations have been considered, set a are the drivers selected because of their period, Set b are series of normal modes and Set c are normal modes with equal mode numbers **??**. The amplitudes for each of the modes has determined using equation (**??**), to use this relation we assume that the 0,0 for the 300s driver has an amplitude of 350m/s (see **?**).

The driver periods for set a correspond to the dominant atmospheric modes of oscillation for example the 5 minute mode and the 3 minute chromospheric mode. The 30s driver was selected because this corresponds to a frequency below that of the atmospheric cutoff and we can use the propagation characteristics as a test of our simulations. The periods for the normal modes were determined for different values of the speed of sound (c_s) in the solar atmosphere at different heights. The periods for the resulting drivers are shown in table **??**.

$$\omega_{nm}^2 = 2\left(\frac{\pi c}{L}\right)^2, \tag{15}$$

Where L is the box length.

$$c_s = \frac{\omega}{k}, \tag{16}$$

With the objective to analyse and understand the nature of the frequency shifts of the excited modes, we consider a number of cases. How wave energy propagation is influenced by the wave modes and frequencies, we compute the time averaged wave energy flux integrated over the cross-sectional area of the simulation box at different heights. The area of integration is perpendicular to the model z axis.

Mode	$c_s = 20km/s$	$c_s = 31.4km/s$
0,0	282.8	180.0
0,1	200.0	127.3
0,2	133.3	84.8
0,3	100.0	63.6

Table 2: Time periods of extended photospheric drivers for normal modes corresponding to c_s at different heights. The first mode number corresponds to the mode for the x-direction and the second number the mode for the y-direction.

Mode	Period (s)
1,1	471.4
2,2	235.7
3,3	157.1

Table 3: Time periods of extended photospheric drivers for normal modes corresponding to equal mode numbers.

$$F_{int} = \frac{1}{t_{max}} \int_0^{t_{max}} \int \mathbf{F_{wave}} \cdot d\mathbf{A}dt, \tag{17}$$

Where the wave energy flux $\mathbf{F_{wave}}$ is given by

$$\mathbf{F_{wave}} = \tilde{\mathbf{p}}_\mathbf{k}\mathbf{v} + \frac{\mathbf{1}}{\mu_\mathbf{0}}(\mathbf{B_b} \cdot \tilde{\mathbf{B}})\mathbf{v} - \frac{\mathbf{1}}{\mu_\mathbf{0}}(\mathbf{v} \cdot \tilde{\mathbf{B}})\mathbf{B_b} \tag{18}$$

We have used the expression for the wave energy flux used by $\tilde{p}_k$ is the perturbed kinetic pressure given by **?**

$$\tilde{p}_k = (\gamma - 1)(\tilde{e} - \frac{(\tilde{\rho} + \rho_b)\mathbf{v}^2}{2} - \frac{\tilde{\mathbf{B}}^2}{2} - \mathbf{B_b} \cdot \tilde{\mathbf{B}}). \tag{19}$$

6. Results of Numerical Simulation

The propagation of waves in a stratified atmosphere can be understood using linearised versions of the equation of continuity, momentum and energy. Such atmospheric waves of expansion have been considered for many years **?**.

Owing to the high gradients, partial reflection of acoustic waves at all frequencies is expected at the transition region. The transition region is the upper boundary of

Mode	Amplitude for 30s	Amplitude for 180s	Amplitude for 300s
0,0	343.4	348.3	350.0
0,1	217.2	220.3	221.4
0,2	153.6	155.8	156.5
0,3	117.8	119.5	120.0

Table 4: Amplitudes of extended photospheric drivers for modes with different driver periods.

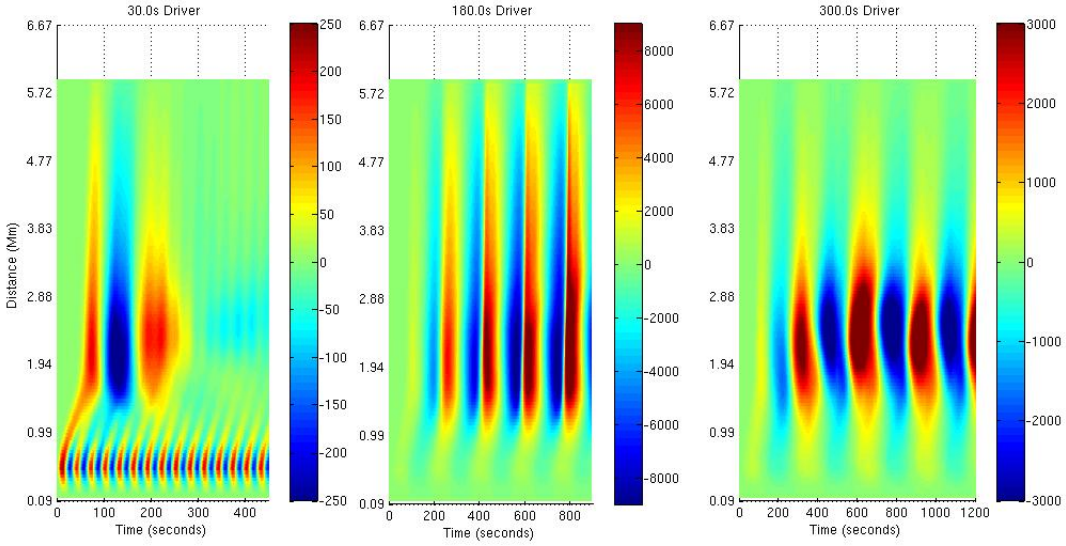

Figure 3: Distance time plot for fundamental model and 30s,180s and 300s driver period for the z component of the velocity for a vertical slice across the box taken at 2Mm and shows the profile of v_z through the solar atmosphere for different time steps (the left hand plot shows the case for the 30s driver, the centre plot the case for the 180s driver and the right hand plot shows the case for the 300s driver).

the chromospheric cavity, it has been previously suggested that this is the source of three-minute transition-region oscillations **?**.

It is known that the propagation of acoustic waves in an unbounded medium is determined by a cut-off period. In a gravitationally stratified atmosphere acoustic waves can only propagate if the wave period is less than the cut off. It was shown that this frequency is a resonance, disturnaces with this frequency trigger a response. Waves with a period greater than the cut-off are evanescent.

The propagation of these acoustic wave modes in a gravitationally stratified atmosphere is determined by characterised cut-off frequencies, theory predicts that waves will only propagate if the wave period is less than the local acoustic cut-off period in the atmosphere.

Following **?** by solving the Klein-Gordon equation for the gravitationally stratified atmosphere (**??**) the cut-off for the atmosphere can be obtained (**??**)

$$\frac{\partial^2 Q}{\partial t^2} - c_s^2(z)\frac{\partial^2 Q}{\partial z^2} + \Omega^2(z)Q = 0, \tag{20}$$

$$P_c(z) = \frac{2\Lambda_0}{c_s(z)}\sqrt{\frac{1}{1+2\frac{d}{dz}\Lambda_0(z)}}, \tag{21}$$

Where the pressure scale height for an atmosphere stratified by a uniform gravitational field is

$$\Lambda_0(z) = \frac{p_0(z)}{g\rho_0(z)}, \tag{22}$$

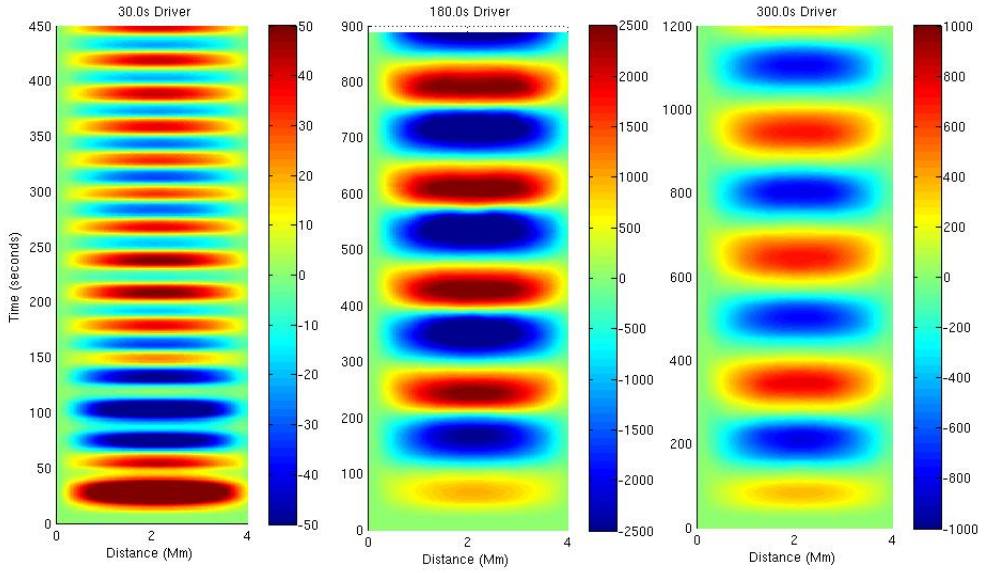

Figure 4: Time-distance plot for fundamental model (0,0) and 30s,180s and 300s driver period for the z component of the velocity for a horizontal slice across the box taken at 0.94Mm shows the profile of v_z across the simulation box at a given point (left hand is 30s driver, centre is 180s driver and the right hand is the 300s driver).

Here $p_0(z)$ and $\rho_0(z)$ are the variation of the equilibrium pressure and density with height. Q is the rescaled velocity perturbation. The variation of the cut-off with solar atmospheric height is shown in figure cutofffrequency$_f ig4 which shows the cut of f period for the V ALIII cat mops here a$

For the fundamental modes (0,0) illustrated in figs. 4, 5 and 6 we observe that there is no significant structure at the transition zone. However, the 30s mode demonstrates the rapid expansion of the perturbation at the penetration height of the the transition region, this is accompanied with an increase in the transverse velocity (v_x) this observationi is true for all 30s, 180s and 300s driver scenarios. As the mode order is increased from $n = 0$, to $n = 1$ and then $n = 2$ its is observed that transition region structuring becomes apparent and is more reminiscent of the observations of **?**.

For the fundamental modes with the 30s, 180s and 300s driver we have plotted distance-time plots of the v_z of the plasma velocity i.e. in the same direction as the driver and in the direction of increasing height through the solar atmosphere. Figure shows the time-distance plots for a vertical section through the simulation box, since this was a fundamental mode the section was taken through the middle of the simulation box. The plots show that the greatest amplitude arises in the transition region in particular for the 180s driver. Looking at the result for the 30s driver it is seen that the initial travelling response reaches a response at around 0.5Mm corresponding to a cut-off of 200s. The maximum amplitude is coherent with the maximum occuring at the same frequency as that of the driver. For the first 70 periods maxima appear in the transition zone. It appears that the transition zone is essentially a source of excitation with freuency lower than that of the driver, however, at longer time periods these motions occur with

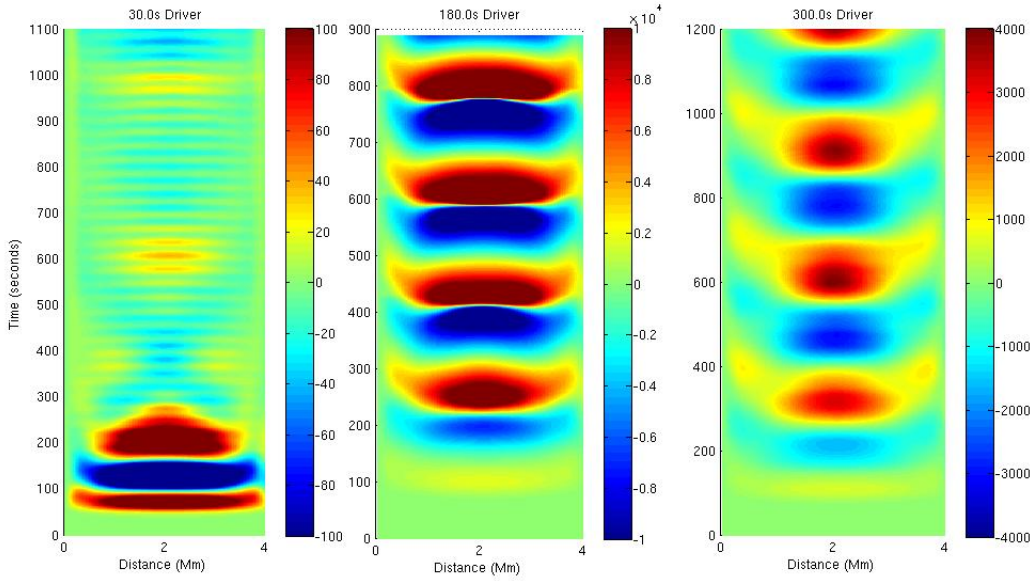

Figure 5: Distance time plot for fundamental model and 30s,180s and 300s driver period for the z component of the velocity for a horizontal slice across the box taken at the transition zone shows the profile of v_z across the simulation box at a height of 2Mm (left hand is 30s driver, centre is 180s driver and the right hand is the 300s driver).

reduced amplitude but with the same period as the driver. For the180s and 300s drivers it is observed that the amplitude in the transition zone is larger than that for the 30s driver by a factor of upto 20. For the 30,180 and 300s case we observe the travelling wave in the Chromosphere and a stationary wave in the solar Corona. Although the 180s mode shows the greatest excitation both the 180s and 300s drivers become evanescent due the the cut-off for the upper atmosphere. Figure shows the distance time plot for a horizontal section taken at a height of 0.94Mm, i.e. through the Chromosphere. The travelling modes in these plots propagate as plane modes with a frequecy consistent with that of the driver. The greatest intensity is observed for the 180s driver. Propagation for the transition zone shown in figure shows the most powerful response for the 180s driver followed by the 300s driver. The response for the 30s driver decays rapidly after the first ten cycles. As we move into the Corona there is further attenuation with the greatest signal reduction for the 30s driver.

The time-distance plots for horizontal sections at an atmospheric height of 4.2Mm are a clear indication of the propagation of waves across the transition zone for the case of the 30s driver it can be seen that the propagation is cut-off after the first 270s of the simulation. All three driver cases indicate a peak with a width of around 90s this peak exhibits a degree of splitting which is most clear for the 300s driver. This effect may be attributable to the superposition of waves reflected from the boundaries of the chromosphere.

Using equation (**??**) we compute the energy flux integral for the range of driver frequencies, modes and at different atmospheric heights. Figure 17 shows the variation

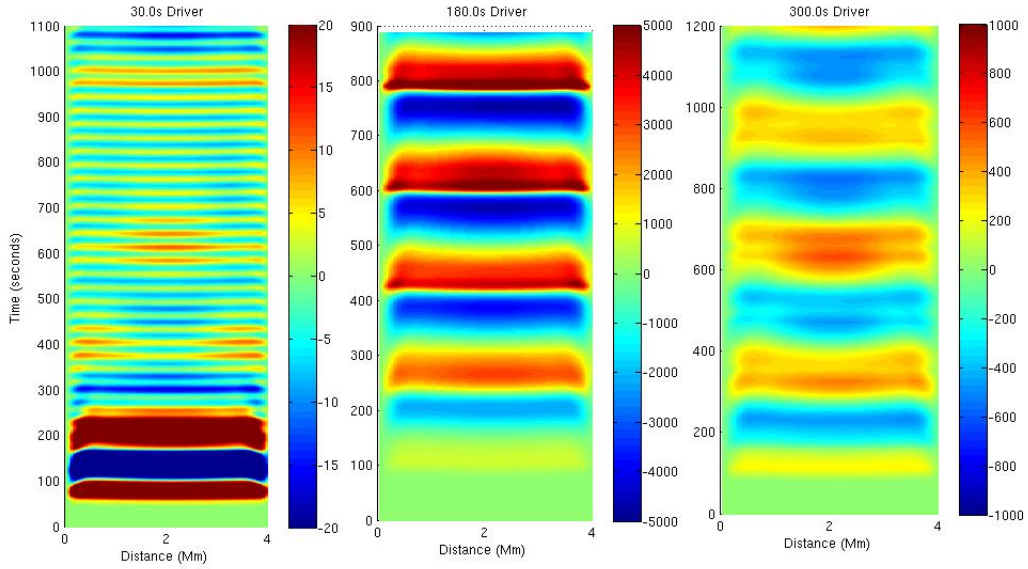

Figure 6: Distance time plot for fundamental model and 30s,180s and 300s driver period for the z component of the velocity for a horizontal slice across the box taken at 4.2Mm shows the profile of v_z across the simulation box (left hand is 30s driver, centre is 180s driver and the right hand is the 300s driver).

of the energy flux ratio, we compute the ratio of the energy flux at a height of 5.5Mm to the driver energy ratio. The figure shows the energy ratios for the different modes. Fitting the data for the (0,0) mode against the power law shown in equation (**??**) gives the values shown in table 12. The powerlaw values are in agreement the values obtained from the observational results of Ireland **?** distinguishing a flat power spectrum for high frequencies and a power spectrum for low frequencies.

$$P(z) = aT^b + c, \tag{23}$$

The results tables show the values of the energy flux from the simulations at different heights. All the modes for the driver periods 180s and 300s are shown as a bar chart in figure 18 and figure 19. For both the 180s and 300s drivers it can be seen that the even modes make the strongest contribution in the corona. The results plotted in figure 20 show the ratio of the Energy flux for models delivering the same quantity of energy to the energy flux for models where the driver amplitude is kept fixed. With the exception of the fundamental mode the ratios appear to be constant for all frequencies suggesting the possibility of using the scaling relation to compute the enrgy flux for differenet frequencies and modes.

Label	Density Profile	Gravity Enabled	Driver
B	VALIIC	yes	single driver at photosphere
C	VALIIC	no	single driver at photosphere
D	constant density	yes	single driver at photosphere
E	constant density	no	single driver at photosphere
F	constant density	no	two drivers at the photosphere and transition zone.

Table 5: Simulations Used to Characterise Oscillatory Motions Arising from the Surface Driver.

	Fitted Values	Ireland (171Å)	Ireland (193Å)
a	-6.199x10^{-9}	$10^{0.57}$	$10^{-0.1}$
b	1.762	1.72	2.2
c	0.002872	10^{-3}	$10^{-3.52}$

Table 6: Power law coefficients for relationship between power and time-period of atmospheric oscillation.

	1Mm	2Mm	4Mm	5.5Mm
30	0.0133	1.7275x10^{-4}	1.0561x10^{-4}	5.5399x10^{-5}
300	0.2607	0.008144	0.002176	0.001119
180	0.7227	0.047895	0.019831	0.010365
435.1	1.9415	0.043601	0.005944	0.003147
179.98	1.6450	0.004502	0.002600	0.001366
282.84	0.1986	0.004007	0.001845	9.7821x10^{-4}

Table 7: (00) mode energy ratio.

	1Mm	2Mm	4Mm	5.5Mm
30	0.0065	1.751x10^{-5}	1.2579x10^{-6}	4.6820x10^{-7}
300	0.1001	8.796x10^{-4}	4.1494x10^{-6}	1.3059x10^{-6}
180	0.1543	5.8381x10^{-4}	3.2715x10^{-5}	1.1343 x10^{-5}
307.1	0.0982	0.001	4.1351x10^{-6}	1.3380 x10^{-6}
127.27	0.0829	4.3190x10^{-4}	5.1387x10^{-5}	2.0397 x10^{-5}
200.0	0.1126	4.4180x10^{-4}	2.0186x10^{-5}	6.3062 x10^{-6}

Table 8: (01) mode energy ratio.

	1Mm	2Mm	4Mm	5.5Mm
30	0.0024	7.2158 x10^{-6}	1.0651x10^{-6}	7.6079x10^{-7}
300	0.0578	4.9604 x10^{-4}	5.5618x10^{-6}	4.1907x10^{-6}
180	0.0687	3.5547 x10^{-4}	6.0675x10^{-5}	4.1492 x10^{-5}
205.1	0.3135	0.0015	1.6520x10^{-4}	1.1272x10^{-4}
84.84	0.0206	5.8903 x10^{-5}1.6520 x10^{-5}	1.1890 x10^{-5}	
133.33	0.0497	1.9731x10^{-4}7.9834 x10^{-5}	5.6267 x10^{-5}	

Table 9: (02) mode energy ratio.

	1Mm	2Mm	4Mm	5.5Mm
30	0.0101	4.2736x10^{-5}	6.3291x10^{-7}	3.7786x10^{-7}
300	0.0359	3.8929x10^{-4}	3.2621x10^{-7}	2.1259x10^{-7}
180	0.0351	1.3948x10^{-4}	3.1342x10^{-6}	1.8205x10^{-6}
153.8	0.0313	1.1043x10^{-4}	3.8071x10^{-6}	2.1034x10^{-6}
63.63	0.0051	9.8989x10^{-6}	7.0207x10^{-7}	4.0621x10^{-7}
100.0	0.0151	3.0678x10^{-5}	2.8527x10^{-6}	1.6707x10^{-6}

Table 10: (03) mode energy ratio .

	1Mm	2Mm	4Mm	5.5Mm
(0,0)	0.7227	0.0479	0.0198	0.0104
(0,1)	0.1543	0.0006	3.2715x10^{-5}	1.1343x10^{-5}
(0,2)	0.0687	0.0004	6.0675x10^{-5}	4.1492x10^{-5}
(0,3)	0.0351	0.0001	3.1342x10^{-6}	1.8205 x10^{-6}
(1,1)	0.4072	0.0011	4.5311x10^{-6}	5.5495x10^{-7}
(1,2)	0.3331	0.0012	3.0728x10^{-6}	1.3055x10^{-6}
(1,3)	0.2961	0.0011	4.8733x10^{-7}	3.4760x10^{-7}
(2,2)	0.3054	0.0011	1.5844x10^{-5}	1.7622x10^{-5}
(2,3)	0.2732	0.0008	2.1443x10^{-6}	1.7045x10^{-6}
(3,3)	0.2205	0.0006	1.9711x10^{-7}	2.6756x10^{-7}

Table 11: 180s driver energy ratio.

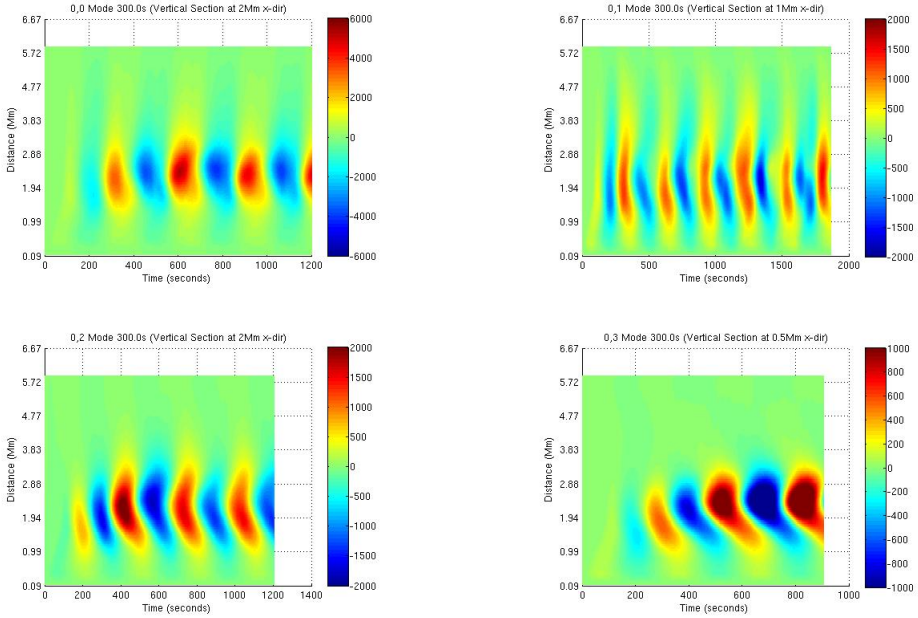

Figure 7: Distance time plot for fundamental model with 300s period for the z component of the velocity. x-direction

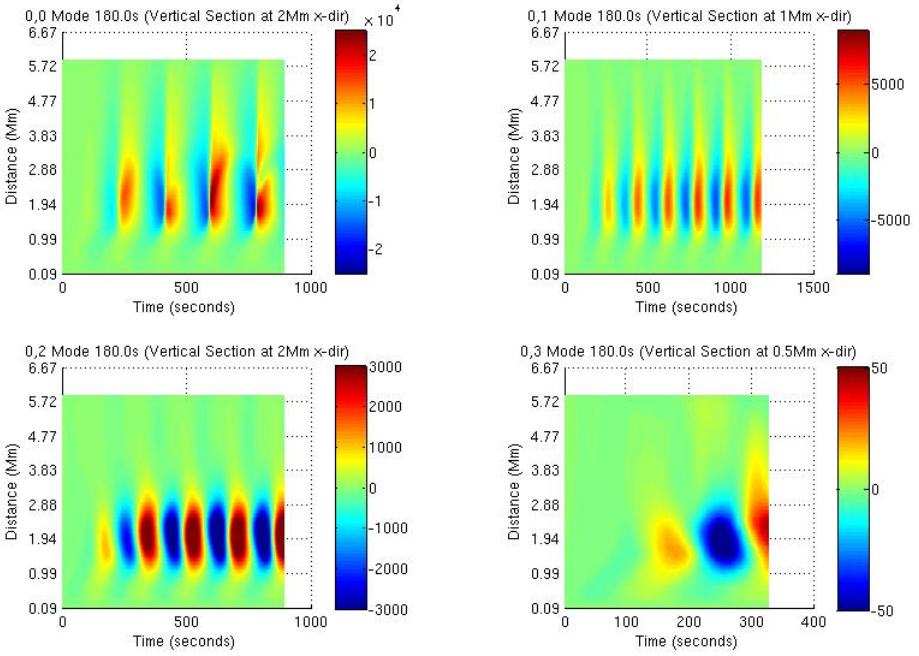

Figure 8: Distance time plot for fundamental model with 180s period for the z component of the velocity. x-direction

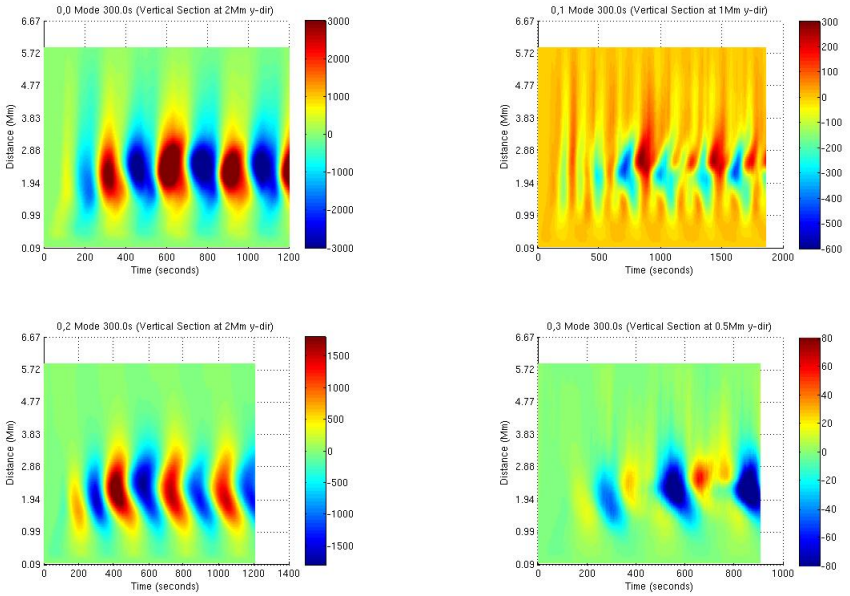

Figure 9: Distance time plot for fundamental model with 300s period for the z component of the velocity. y-direction

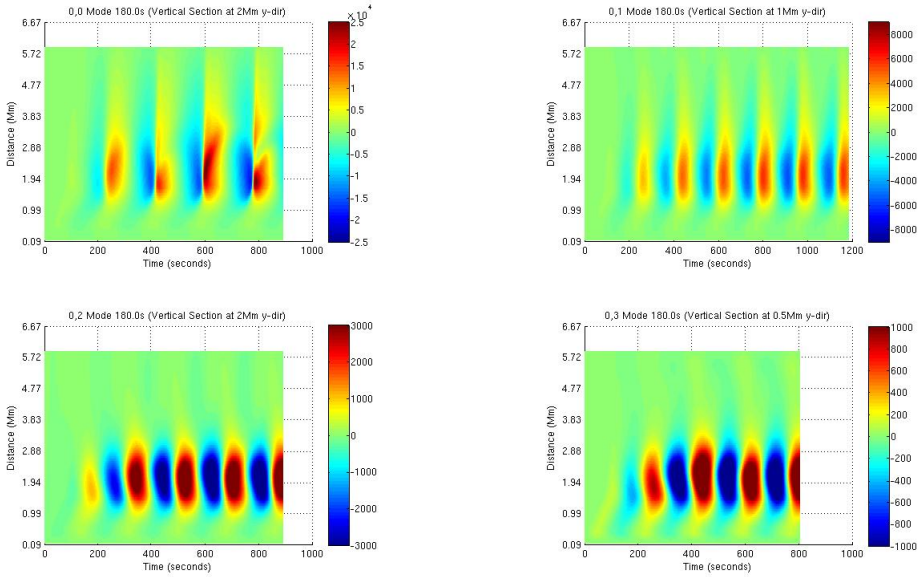

Figure 10: Distance time plot for fundamental model with 180s period for the z component of the velocity. y-direction

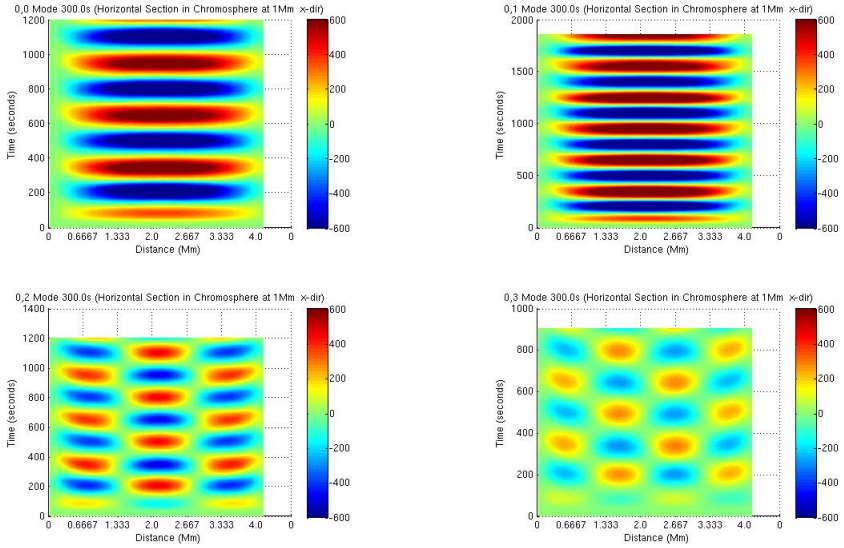

Figure 11: Distance time plot for modes with 300s period Horizontal Section through the Chromosphere (at 1Mm) for the z component of the velocity. x-direction

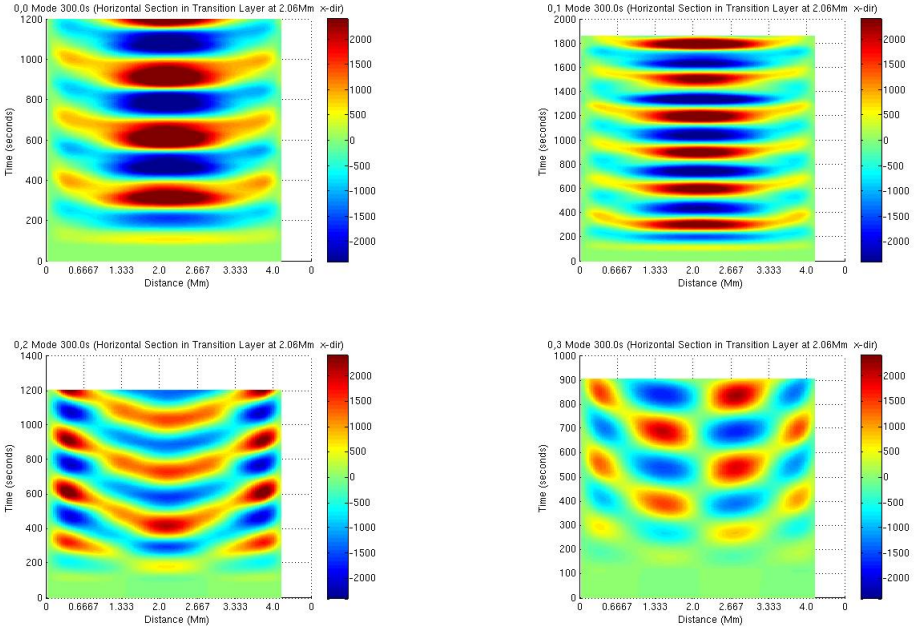

Figure 12: Distance time plot for modes with 300s period Horizontal Section through the Transition Region (at 2.06Mm) for the z component of the velocity. x-direction

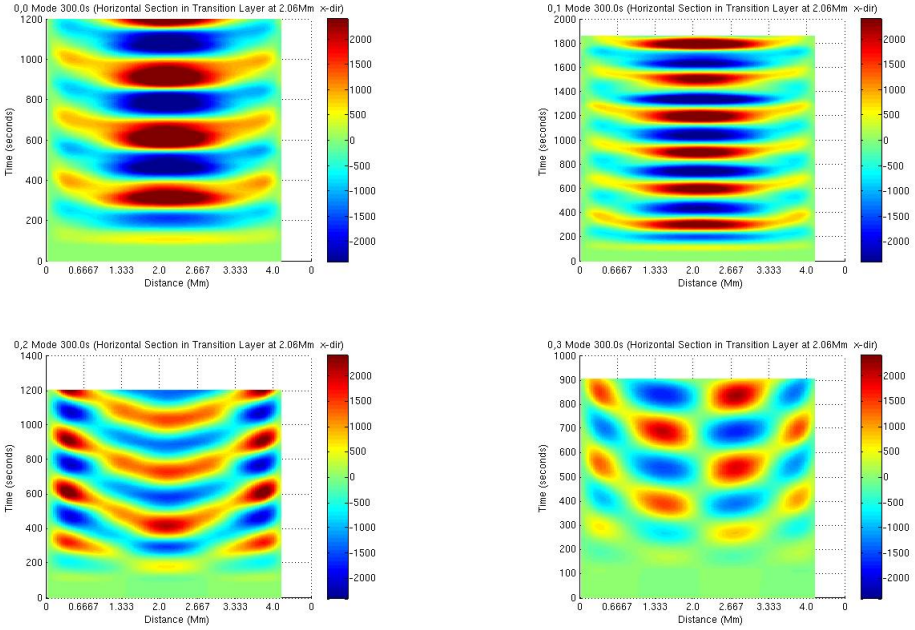

Figure 13: Distance time plot for modes with 300s period Horizontal Section through the Solar Corona (at 4.3Mm) for the z component of the velocity. x-direction

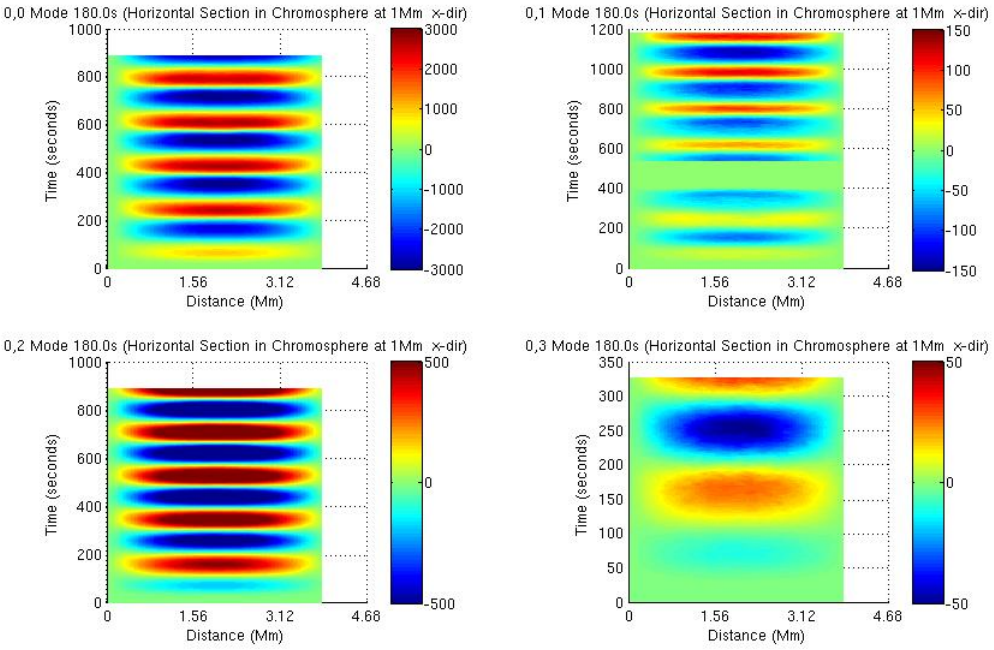

Figure 14: Distance time plot for modes with 180s period Horizontal Section through the Chromosphere (at 1Mm) for the z component of the velocity. x-direction

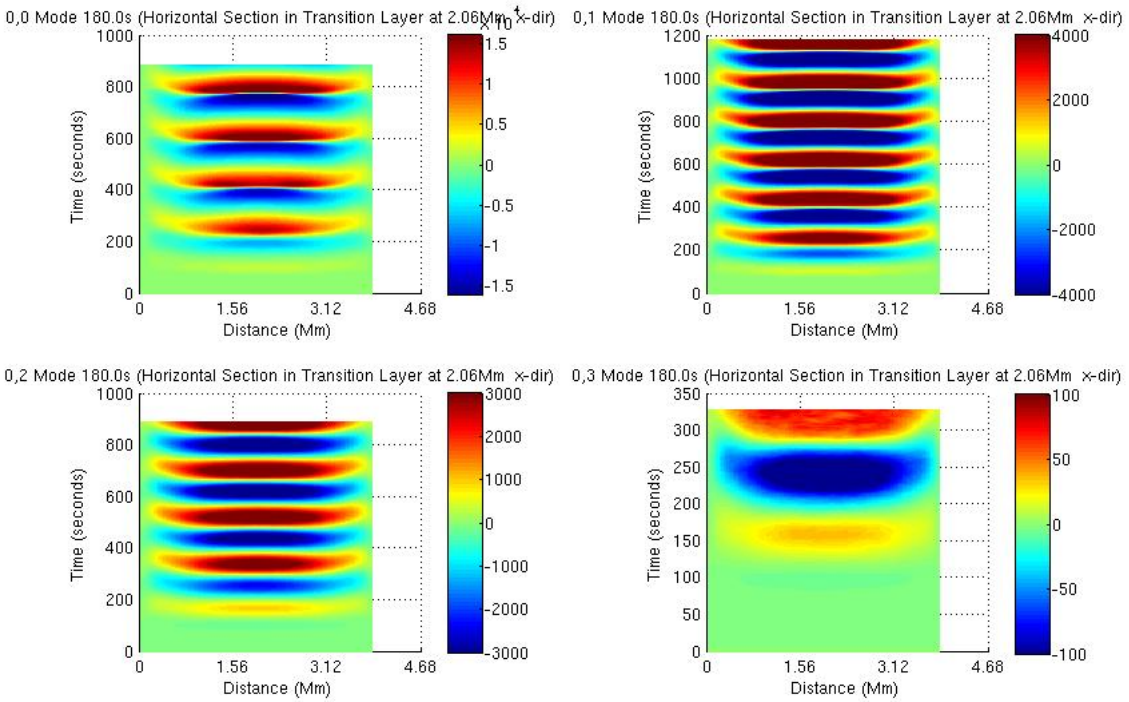

Figure 15: Distance time plot for modes with 180s period Horizontal Section through the Transition Region (at 2.06Mm) for the z component of the velocity. x-direction

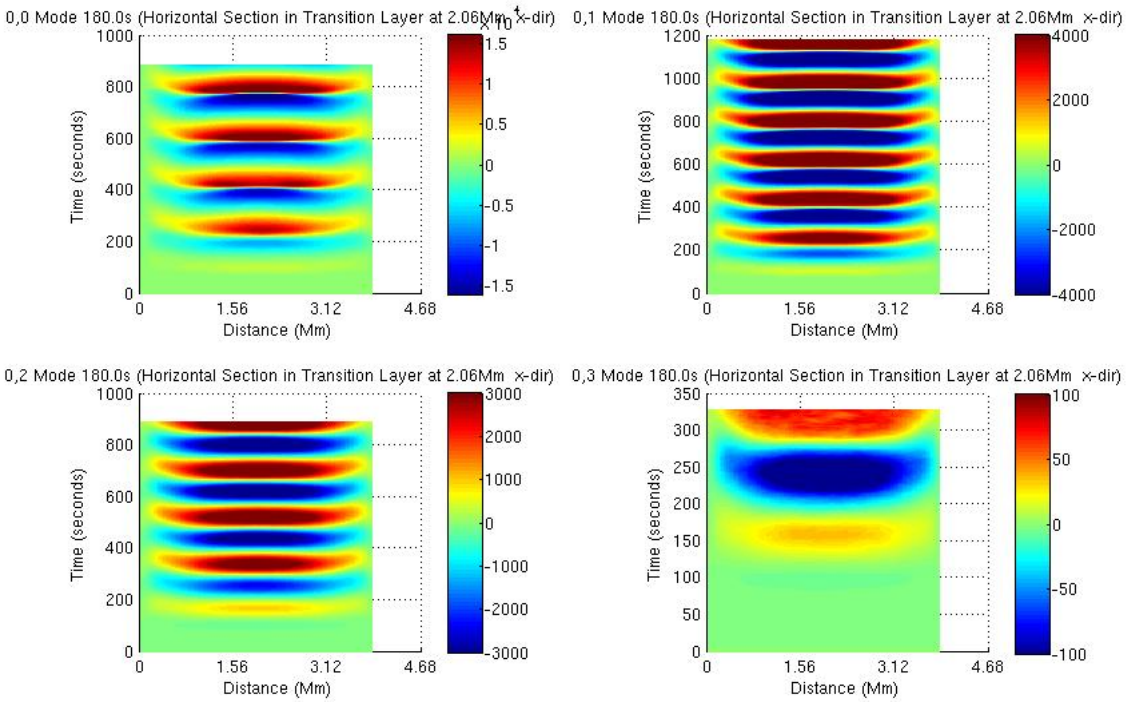

Figure 16: Distance time plot for modes with 180s period Horizontal Section through the Solar Corona (at 4.3Mm) for the z component of the velocity. x-direction

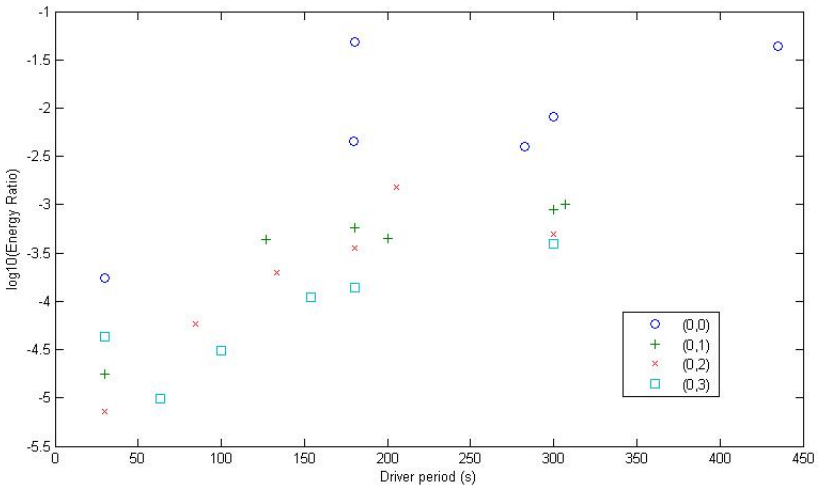

modes$_5$p5$Mm.jpg$

Figure 17: Variation of Energy Flux Ratio with the Driver Energy at a Height of 5.5Mm for a Solar Atmosphere Excited with a p-Mode Driver Located at a Height of 50km

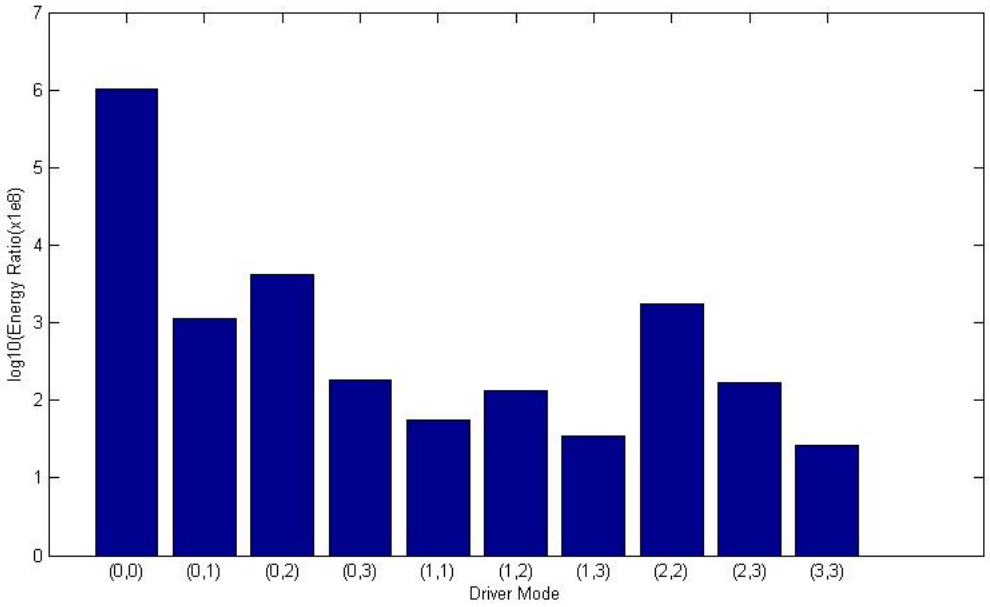

Figure 18: Variation of Energy Flux Ratio at a Height of 5.5Mm for a Solar Atmosphere Excited with a 180s p-Mode Driver Located at a Height of 50km

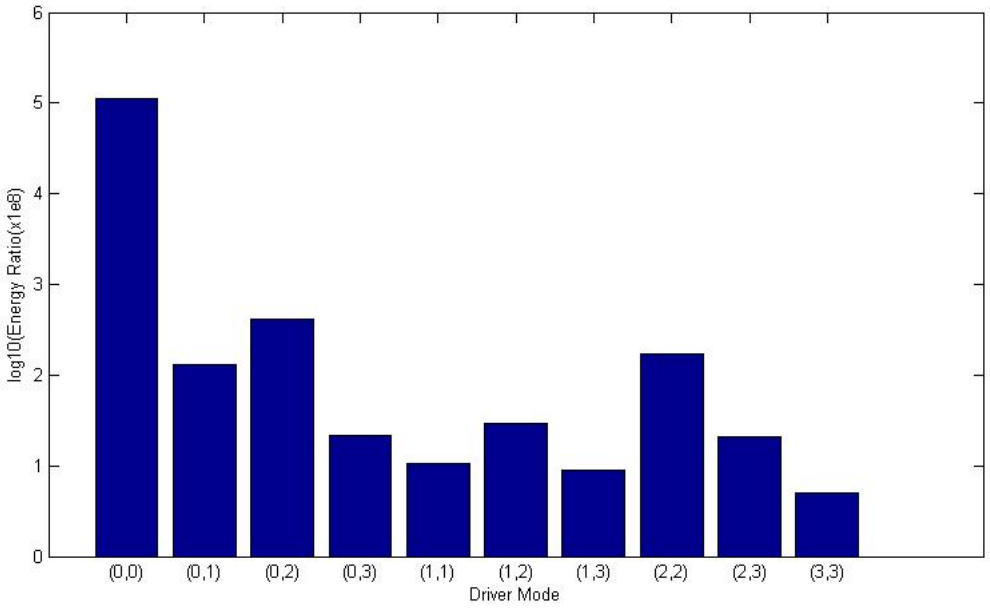

Figure 19: Variation of Energy Flux Ratio at a Height of 5.5Mm for a Solar Atmosphere Excited with a 300s p-Mode Driver Located at a Height of 50km

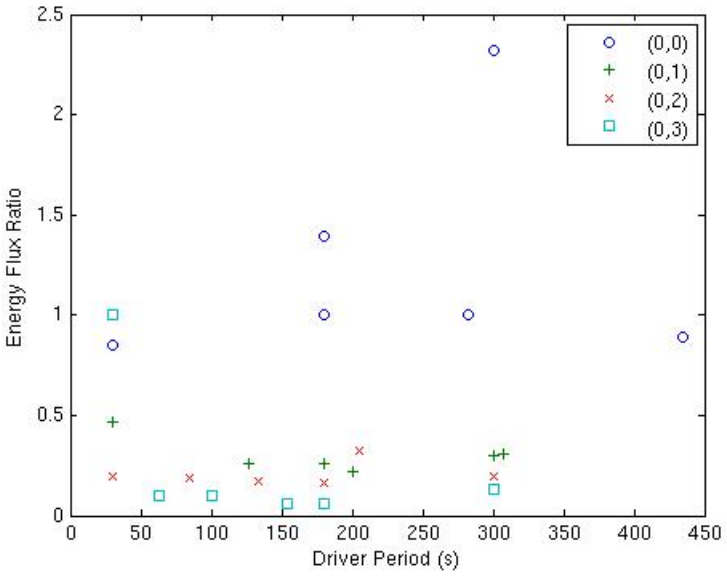

modes$_5$p5$Mm.jpg$

Figure 20: Variation of Energy Flux Ratio at a Height of 5.5Mm for a Solar Atmosphere Excited with a p-Mode Driver Located at a Height of 50km

7. Conclusions

Our results support the notion that solar global oscillations are a driver for a range of global dynamical phenomena resulting in atmospheric and chr0mospheric oscillations which contribute to the propagation of energy into the solar atmosphere. Global dynamical phenomena arise from a range of sources including solar global oscillations, turbulent motions from convective cells and nano flares giving the possibility of continuous reconnection events.

1. The consistency of the frequency dependence of the energy flux for our numerical simulations and powel flux measurements obtained from SDO supports the use of numerical simulations for modelling the excitations driven by solar global oscillations for the quiet sun.
2. Agreement between the energy flux predictions of our numerical simulations and the the two layer Klein-Gordon model supports
3. Energy propgation into the atmosphere occurs for a range of frequencies and may explain observed intensity oscillations for periods greater than the well known 3 minute and 5 minute oscillations.
4. Energy flux propagation into the solar corona is strongly dependent on the wave modes

RE acknowledges M. Kéray for patient encouragement and is also grateful to NSF, Hungary (OTKA, Ref. No. K83133). The authors thank the Science and Technology

Facilities Council (STFC), UK for the support they received. We acknowledge Corporate Information and Computing Services at The University of Sheffield for the provision of the High Performance Computing Service.

8. References

References

Beck, C., Rezaei, R., Puschmann, K. G., Aug. 2012. The energy of waves in the photosphere and lower chromosphere. II. Intensity statistics. A&A544, A46.

Carlsson, M., Stein, R. F., Feb. 1995. Does a nonmagnetic solar chromosphere exist? ApJL440, L29–L32.

Caunt, S. E., Korpi, M. J., Apr. 2001. A 3D MHD model of astrophysical flows: Algorithms, tests and parallelisation. A&A369, 706–728.

De Moortel, I., Dec. 2005. An overview of coronal seismology. Philosophical Transactions of the Royal Society of London Series A 363, 2743–2760.

Griffiths, M. K., Fedun, V., Erdélyi, R., Mar. 2015. A Fast MHD Code for Gravitationally Stratified Media using Graphical Processing Units: SMAUG. Journal of Astrophysics and Astronomy 36, 197–223.

Ireland, J., McAteer, R. T. J., Inglis, A. R., Jan. 2015. Coronal Fourier Power Spectra: Implications for Coronal Seismology and Coronal Heating. ApJ798, 1.

Jefferies, S. M., McIntosh, S. W., Armstrong, J. D., Bogdan, T. J., Cacciani, A., Fleck, B., Oct. 2006. Low-frequency magneto-acoustic waves in the solar chromosphere. In: Proceedings of SOHO 18/GONG 2006/HELAS I, Beyond the spherical Sun. Vol. 624 of ESA Special Publication. p. 16.1.

Kalkofen, W., Feb. 2012. The Validity of Dynamical Models of the Solar Atmosphere. Sol. Phys.276, 75–95.

Kalkofen, W., Rossi, P., Bodo, G., Massaglia, S., Sep. 2010. Acoustic waves in a stratified atmosphere. IV. Three-dimensional nonlinear hydrodynamics. A&A520, A100.

Lamb, H., 1932. Hydrodynamics.

Leenaarts, J., Carlsson, M., Hansteen, V., Gudiksen, B. V., Jun. 2011. On the minimum temperature of the quiet solar chromosphere. A&A530, A124.

Leibacher, J. W., Stein, R. F., 1971. A New Description of the Solar Five-Minute Oscillation. 7, 191–192.

Leighton, R. B., 1960. In: Thomas, R. N. (Ed.), Aerodynamic Phenomena in Stellar Atmospheres. Vol. 12 of IAU Symposium. pp. 321–325.

Lites, B. W., Kubo, M., Socas-Navarro, H., Berger, T., Frank, Z., Shine, R., Tarbell, T., Title, A., Ichimoto, K., Katsukawa, Y., Tsuneta, S., Suematsu, Y., Shimizu, T., Nagata, S., Jan. 2008. The Horizontal Magnetic Flux of the Quiet-Sun Internetwork as Observed with the Hinode Spectro-Polarimeter. ApJ672, 1237–1253.

Malins, C., Oct. 2007. On transition region convection cells in simulations of {p}-mode propagation. Astronomische Nachrichten 328, 752–755.

McWhirter, R. W. P., Thonemann, P. C., Wilson, R., Apr. 1975. The heating of the solar corona. II - A model based on energy balance. A&A40, 63–73.

Murawski, K., Zaqarashvili, T. V., Sep. 2010. Numerical simulations of spicule formation in the solar atmosphere. A&A519, A8.

Roberts, B., Edwin, P. M., Benz, A. O., Apr. 1984. On coronal oscillations. ApJ279, 857–865.

Shelyag, S., Fedun, V., Erdélyi, R., Aug. 2008. Magnetohydrodynamic code for gravitationally-stratified media. A&A486, 655–662.

Taroyan, Y., Erdélyi, R., Sep. 2008. Global Acoustic Resonance in a Stratified Solar Atmosphere. Sol. Phys.251, 523–531.

Ulrich, R. K., Dec. 1970. The Five-Minute Oscillations on the Solar Surface. ApJ162, 993.

Vernazza, J. E., Avrett, E. H., Loeser, R., Apr. 1981. Structure of the solar chromosphere. III - Models of the EUV brightness components of the quiet-sun. 45, 635–725.